Bioactive Materials 35 (2024) 56–66

Contents lists available at ScienceDirect

Bioactive Materials

journal homepage: www.keaipublishing.com/en/journals/bioactive-materials

Accelerated corrosion of 316L stainless steel in a simulated oral environment via extracellular electron transfer and acid metabolites of subgingival microbiota

Ying Zheng [a], Yi Yang [b,c], Xianbo Liu [a], Pan Liu [b,c], Xiangyu Li [b,c], Mingxing Zhang [b,c], Enze Zhou [b,c], Zhenjin Zhao [a], Xue Wang [a], Yuanyuan Zhang [a], Bowen Zheng [a], Yuwen Yan [a], Yi Liu [a,**], Dake Xu [b,c,d,*], Liu Cao [e,f,***]

[a] School and Hospital of Stomatology, China Medical University, Liaoning Provincial Key Laboratory of Oral Diseases, Shenyang, China
[b] Shenyang National Laboratory for Materials Science, Northeastern University, Shenyang, China
[c] State Key Laboratory of Rolling and Automation, Northeastern University, Shenyang, China
[d] Electrobiomaterials Institute, Key Laboratory for Anisotropy and Texture of Materials (Ministry of Education), Northeastern University, Shenyang, China
[e] College of Basic Medical Sciences, Key Laboratory of Medical Cell Biology, Ministry of Education, China Medical University, Shenyang, China
[f] Institute of Health Sciences, China Medical University, Shenyang, China

ARTICLE INFO

Keywords:
Oral subgingival microbiota
316L SS
Corrosion
Extracellular electron transfer
Acid metabolites

ABSTRACT

316L stainless steel (SS) is widely applied as microimplant anchorage (MIA) due to its excellent mechanical properties. However, the risk that the oral microorganisms can corrode 316L SS is fully neglected. Microbiologically influenced corrosion (MIC) of 316L SS is essential to the health and safety of all patients because the accelerated corrosion caused by the oral microbiota can trigger the release of Cr and Ni ions. This study investigated the corrosion behavior and mechanism of subgingival microbiota on 316L SS by 16S rRNA and metagenome sequencing, electrochemical measurements, and surface characterization techniques. Multispecies biofilms were formed by the oral subgingival microbiota in the simulated oral anaerobic environment on 316L SS surfaces, significantly accelerating the corrosion in the form of pitting. The microbiota samples collected from the subjects differed in biofilm compositions, corrosion behaviors, and mechanisms. The oral subgingival microbiota contributed to the accelerated corrosion of 316L SS via acidic metabolites and extracellular electron transfer. Our findings provide a new insight into the underlying mechanisms of oral microbial corrosion and guide the design of oral microbial corrosion-resistant materials.

1. Introduction

Microbiologically influenced corrosion (MIC) is a bioelectrochemical process, which is initiated and facilitated by biofilms, resulting from complex interactions among microorganisms, environments, and materials [1,2]. As a result of breathing and swallowing, the oral cavity environment is exposed to a vast array of microbes, including more than 700 species of bacteria, fungi, archaea, viruses, and protozoa [3–5]. With the continuous development of oral science and technology, metal materials are widely used in orthodontics, prosthodontics, and implantology [6]. In recent, with the widespread application of dental metal materials, oral MIC has become an emerging hot topic for scholars in material science and dentistry [7–11].

At present, orthodontic treatment has been commonly used clinically for dental malformation, while the efficacy depends on anchorage reinforcement [12]. Anchorage in the orthodontic process is to withstand the reaction force caused by the movement of the orthodontic teeth to firmly pull the teeth that need to be moved to the appropriate

Peer review under responsibility of KeAi Communications Co., Ltd.
* Corresponding author. Shenyang National Laboratory for Materials Science, Northeastern University, Shenyang, China.
** Corresponding author. School and Hospital of Stomatology, China Medical University, Liaoning Provincial Key Laboratory of Oral Diseases, Shenyang, China.
*** Corresponding author. College of Basic Medical Sciences, Key Laboratory of Medical Cell Biology, Ministry of Education, China Medical University, Shenyang, China.
E-mail addresses: liuyi@cmu.edu.cn (Y. Liu), xudake@mail.neu.edu.cn (D. Xu), lcao@cmu.edu.cn (L. Cao).

https://doi.org/10.1016/j.bioactmat.2024.01.007
Received 16 October 2023; Received in revised form 26 December 2023; Accepted 8 January 2024

position. Microimplant anchorage (MIA), as a novel class of anchorage, has been rapidly developed and increasingly common for clinical application due to its essential characteristics for stable and reliable operation and low compliance requirements for adolescents [13]. The application of MIA has simplified the treatment of many complicated cases, such as mass retraction, occlusal plane correction, tooth intrusion or uprighting [14]. Generally, two commonly utilized materials for MIA in clinical practice are titanium alloy and 316L SS. While titanium alloy exhibits favorable biocompatibility and corrosion resistance, its drawbacks lie in its relatively lower hardness and comparatively higher cost [12–14]. Conversely, 316L SS is extensively employed in clinical due to its balance of mechanical properties, corrosion resistance, and cost [12–14]. When the MIA is implanted clinically, a part of the MIA is exposed in the oral cavity to facilitate orthodontic force application, and the other part is implanted through periodontal tissue to the alveolar bone to maintain anchorage. This implantation method leads to a large area of contact with the oral microbial flora and the MIA material, especially the neck of the MIA, which enriches a large amount of subgingival flora. It is well known that the attached biofilms mainly contribute to MIC. However, the potential concern that subgingival microbial flora can corrode MIA made of 316L SS is fully neglected. Currently, limited research has been done in the field of MIC caused by oral microorganisms, of which most existing studies focused mainly on individual bacterial strains [8,10,11]. The MIC caused by real oral microbiota has been rarely reported in the past decade [15]. MIA-MIC caused by the subgingival microbial flora is still in the blank stage.

According to bioenergetics, MIC is divided into extracellular electron transfer MIC (EET-MIC) and metabolite MIC (M-MIC) [16–19]. EET-MIC requires biocatalysis by the biofilms, which uptake the electrons released from the metal matrix and transfer them into the cells via direct and/or mediated pathways, resulting in the occurrence of corrosion [1]. M-MIC occurs outside the cell without required bioactivation and is triggered by acidic or corrosive metabolites secreted by bacteria [1]. EET-MIC is more likely to cause pitting corrosion, while M-MIC appears to have uniform corrosion [1,7–11,16–19]. Corrosion in the oral environment will cause a large amount of metal ions to dissolve and affect local oral health and then enter the body with swallowing, resulting in potential systemic health risks [11,17]. 316 L SS has become the mainstream material for MIA due to its excellent mechanical properties and great resistance to breakage and penetration capability [14]. Therefore, the corrosivity of 316L SS caused by the subgingival microbial flora should be evaluated and the underlying MIC mechanisms are desired.

This study aims to investigate the behaviors and mechanisms of oral subgingival microbiota on the corrosion of 316L SS in a simulated oral environment in vitro. Surface characterization and electrochemical measurements were used to examine the biofilm's corrosivity. 16S rRNA and metagenome sequencing analyses provided insights into the subgingival microbial community and the underlying MIC mechanisms. Herein, we found that multispecies biofilms formed and attached onto 316L SS surfaces, significantly accelerated the corrosion of 316L SS via acidic metabolites and extracellular electron transfer.

2. Materials and methods

2.1. Material

The chemical composition of 316L SS is shown in Table S1. 316L SS was cut into square coupons of 10 mm × 10 mm × 2 mm, and the surface was abraded with 240#, 400#, 600#, 800#, and 1000# SiC sand papers, respectively. The coupons for electrochemical experiments and metallic ions release detection were embedded in epoxy resin, leaving only an exposed surface area of 10 mm × 10 mm.

2.2. Preparation of biofilms

Microbiota samples were randomly collected from the patients who needed MIAs for orthodontic treatment at China Medical University Stomatological Hospital. This study was approved by the Local Committee for Bioethics (approval number 2021-17), and informed consent was obtained from all subjects. All patients were informed of the need for MIAs combined with fixed appliances during the pretreatment planning stage. All MIAs were implanted in the buccal maxillary molar region. When clinical treatment was finished, MIAs were removed by the sterile MIA screwdriver and placed into a 100 mL brain-heart infusion (BHI) broth medium. After anaerobic culture at 37 °C for 1 day, the microbiota was preserved as the initial inoculation.

The artificial saliva used in this work was composed of (mg/L) NaCl 125.6, KCl 963.9, KH_2PO_4 654.5, Na_2SO_4 336.6, NH_4Cl 178, urea 200, $NaHCO_3$ 630.8 and $CaCl_2$ 172. To simulate the natural oral environment, 4 g/L yeast and 2 g/L glucose were added into the simulated saliva as carbon source, organic nitrogen, and growth factors. The final pH value of the medium was adjusted to 6.8 ± 0.1 with sterile phosphoric acid. High purity nitrogen was sparged into the medium for 40 min to remove dissolved oxygen.

The immersion test was conducted in a 50 mL conical flask with 40 mL artificial saliva, following incubation to an optical density (OD) 0.4 at $\lambda_{600\ nm}$. Electrochemical experiments were carried out anaerobically in a 500 mL glass cell with 300 mL medium at 37 °C for 7 days.

2.3. Biofilm and coupon surface morphologies

After 7 days of immersion, the planktonic bacteria were removed by PBS washing, and biofilms on coupons were fixed in 2.5 % glutaraldehyde for 4 h and then dehydrated in a gradient of ethanol solutions. Then, the samples were sputter-coated with gold and observed by field emission scanning electron microscopy (FESEM, Ultra-Plus, Zeiss, Germany).

After incubation for 7 days, the planktonic bacterial cells were washed with PBS, and the biofilm was stained with SYTO9 and propidium iodide (PI) for 20 min. Six fields were randomly selected to observe the biofilms by confocal scanning microscopy (CLSM, C2 Plus, Nikon, Japan).

According to the American Society for Testing and Materials (ASTM) standard (G1-03), chemical cleaning procedures were performed to remove surface corrosion products. The pitting morphologies were visualized under another CLSM (LEXT OLS4100, Olympus, Japan).

2.4. Electrochemical tests

To evaluate the corrosion behavior of oral microbiota on 316L SS, an electrochemical workstation (Reference 600, Gamry Instruments, Inc., USA) was used to perform the electrochemical tests. 316L SS electrode served as the working electrode, the counter electrode was platinum, and the reference electrode was a saturated calomel electrode. The open circuit potential (OCP), linear polarization resistance (LPR), and potential dynamic polarization data were measured. LPR measurements were run at a potential scan rate of 0.125 mV/s and a potential range of −10 to 10 mV versus the E_{OCP}. The corrosion potential and current density were determined by potentiodynamic polarization scanning on day 7, which was performed at a scan rate of 0.333 mV/s from −500 mV to 800 mV vs. E_{OCP}. All the electrochemical tests were at least repeated thrice to guarantee the reproducibility.

2.5. pH, riboflavin, organic acid concentrations, detection of metal ions and Griess assay

Throughout the experiment, the values of pH (Five Easy plus, Mettler Toledo, Switzerland) were recorded daily. Concentrations of extracellular riboflavin and organic acids (propionic acid, succinic acid, citric

acid, acetic acid, lactic acid, malonic acid, malic acid, formic acid, tartaric acid, oxalic acid) were measured by HPLC (UltiMate 3000, Thermo Scientific, USA) after 7 days of immersion. The concentrations of metal ions (Fe, Ni, Cr, Mo) were measured by atomic absorption spectrometry (Z-2000, Hitachi, Japan), and then the results were converted to concentration per unit area (ng cm^{-2}). Anions (including NO_3^-, Cl^-, SO_4^{2-}, and PO_4^{3-}) were quantified from the medium using an ion chromatograph (ICS-5000, Thermo Scientific Dionex, USA). After microbiota samples were co-cultured with 316L SS for 7 days, 10 g/L KNO_3 was added for another 1 h of culture. Media were mixed with Griess reagent, and OD was measured at $\lambda_{540\ nm}$ for the Griess assay.

2.6. XPS and AES measurements

The coupons were removed from the vials in the anaerobic chamber after 7 days of coculture, washed with deionized water and dried. The X-ray photoelectron spectroscopy (XPS) and Auger electron spectroscopy (AES) experiments were conducted using an XPS microprobe (Esca-Lab250Xi, Thermo, USA) and a scanning Auger microscope (PHI 710, ULVAC-PHI, Japanese), respectively. For XPS measurement, a monochromatic AI Kα X-ray source (1500 eV energy and 150 W power) was used within 50 eV pass energy with a step size of 0.2 eV.

2.7. FIB-SEM/TEM analysis

Coupons with attached biofilms for FIB-SEM and transmission electron microscopy (TEM) observation were prepared as described in the above section. After observation by FESEM with a focused ion beam system (FIB, Helios NanoLab 460HP, FEI), the location of the FIB-TEM slice was determined. High-angle annular dark-field (HAADF) imaging

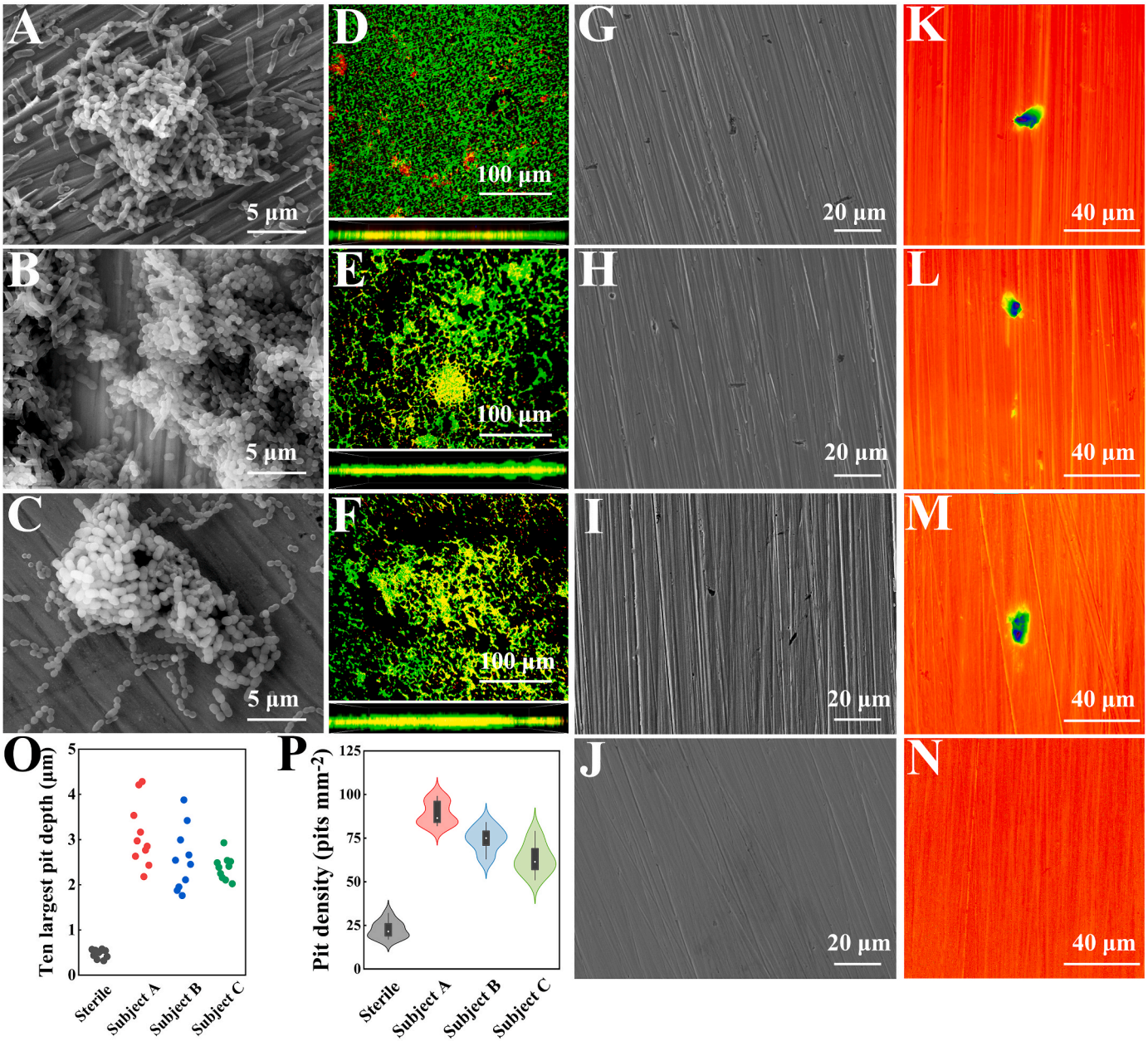

Fig. 1. SEM and CLSM images of biofilm and pit morphology on 316L SS surface. Biofilm formation after 7 days: (A) subject A; (B) subject B; (C) subject C. CLSM images of biofilms with live/dead stain: (D) subject A; (E) subject B; (F) subject C. SEM analysis on the 316 L SS surfaces after removing the biofilms and corrosion products: (G) subject A; (H) subject B; (I) subject C; (J) sterile medium. CLSM images of pits on 316L SS surfaces: (K) subject A; (L) subject B; (M) subject C; (N) sterile medium. Analyses of pit depth (O) and pit density (P).

and energy dispersive spectrometer (EDS) mapping were acquired by a TEM (FEI Talos F200X).

2.8. 16S rRNA and metagenome sequencing

The planktonic and sessile bacterial cells after 7 days of incubation with 316 L SS coupons were analyzed by 16S rRNA sequencing. The hypervariable region V3–V4 of the bacterial 16S rRNA gene was amplified with primer pairs 338F (5′-ACTCCTACGGGAGGCAGCAG-3′) and 806R (5′-GGACTACHVGGGTWTCTAAT-3′) by an ABI GeneAmp® 9700 PCR thermocycler (ABI, CA, USA). After PCR amplification and purification, the 16S rRNA gene was sequenced on an Illumina MiSeq PE300 platform (Illumina, San Diego, USA). Raw 16S rRNA gene sequencing reads were demultiplexed, quality-filtered by fastp (v 0.20.0), and merged by FLASH (v 1.2.7). Operational taxonomic units (OTUs) were clustered with a 97 % similarity cutoff using UPARSE (v 7.1), and chimeric sequences were identified and deleted. The taxonomy of each OTU representative sequence was analyzed by RDP Classifier (V

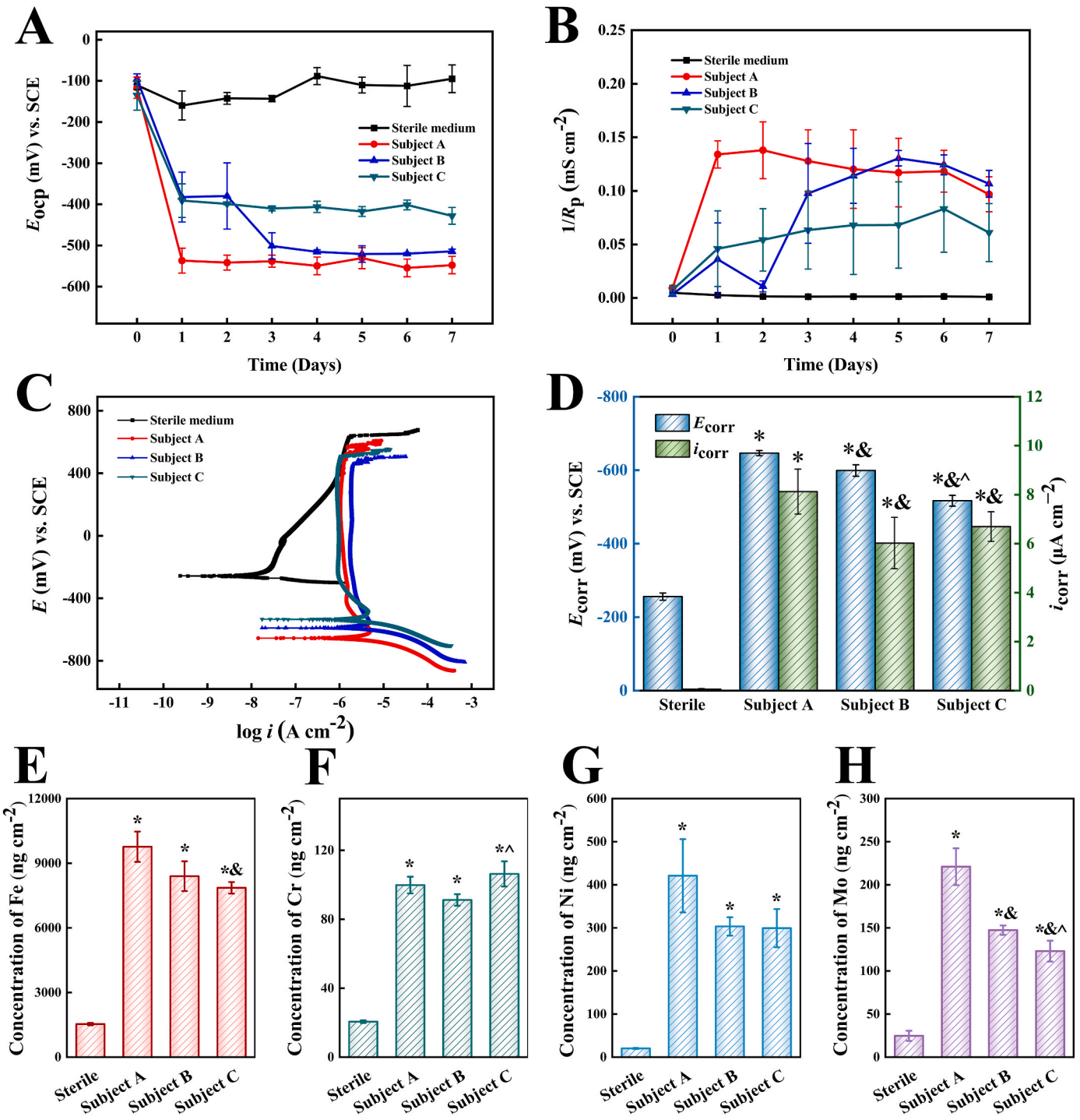

Fig. 2. Electrochemical analyses and concentrations of metallic ions released from the 316L SS coupons after immersion in the different media for 7 days: (A) open circuit potential over time; (B) 1/Rp over time; (C) the potentiodynamic polarization curves of 316L SS after exposure to different media; (D) fitted corrosion parameters obtained from potentiodynamic polarization curves. Concentrations of metallic ions release: (E) Fe; (F) Cr; (G) Ni; (H) Mo. *: versus to sterile, $p < 0.05$; &: versus to subject A, $p < 0.05$; ^: versus to subject B, $p < 0.05$.

2.2) against the silva138/16s_bacteria database (70 % cutoff).

Total genomic DNA was extracted from the three biofilm samples. For paired-end library construction, the DNA extract was fragmented to an average size of approximately 400 bp using Covaris M220 (Gene Company Limited, China). A paired-end library was constructed using NEXTFLEX® Rapid DNA-Seq (Bioo Scientific, Austin, TX, USA), and paired-end sequencing was performed on Illumina NovaSeq (Illumina Inc., San Diego, CA, USA).

3. Results

3.1. Morphology of biofilms and pitting observation

We observed the biofilm formation of sessile cells on the 316 L SS surface after 7 days of coculture (Fig. 1A–C). From the SEM images, complex and tunable multilayered microstructures can be observed in the biofilms from three subjects. A loose biofilm composed of rod-shaped and streptococcal bacteria was observed in subject A. In contrast, a thick and dense bacterial consortium derived from the shaped and globule bacteria was embedded in the biofilm of subject B. The microbial flora containing globular, short rod-shaped, double globular, and ball-shaped bacteria appeared as clusters on the surface of subject C. We used CLSM to observe the biofilm thickness and different survival states of bacteria in the same environment among different subjects (Fig. 1D–F). The dead bacteria exhibited a diffuse distribution with a punctate pattern in the biofilm of subject A but aggregated into clumps on the 316L SS surfaces collected from subjects B and C. The thickest biofilm was 44.8 ± 2.4 μm for subject B, followed by 37.6 ± 3.6 μm for subject C. Subject A showed the thinnest and most evenly distributed biofilm with the thickness of 35.0 ± 0.5 μm.

After removing the biofilm and corrosion products, pits on the coupon surface were examined under SEM (Fig. 1G–J) and CLSM (Fig. 1K-N). No obvious corrosion was detected in the sterile system, whereas extensive pitting corrosion was found on the surface of coupons in the presence of microbiota collected from subjects A, B, and C, indicating that 316 L SS suffered a more severe pitting in the presence of oral microbiota than the abiotic sterile control. The statistics of pit depth and density in Fig. 1O and P directly reflected that the 316L SS were susceptible to pitting corrosion caused by the oral biofilm. The biofilm of subject A caused the most severe pitting corrosion, with an average pit density of 89.2 pits mm^{-2} and the largest pit depth of 4.28 μm. The average pit depth of subject A (3.02 ± 0.72 μm) was also larger than that of subject B (2.55 ± 0.71 μm) and subject C (2.38 ± 0.26 μm).

3.2. Analyses of electrochemical measurements, metal ions release, and corrosion products

As shown in Fig. 2A and B, E_{OCP} and $1/R_p$ of samples in the sterile medium showed no evident change over time, demonstrating that 316L SS was almost not corroded in the anaerobic abiotic medium. E_{OCP} in the presence of oral microbiota all shifted negatively, and subject A reached the lowest E_{OCP} value of −540 mV. $1/R_p$ values in the presence of microbiota increased significantly after 1 day of immersion. The potential dynamic polarization curves and obtained corresponding corrosion parameters of different culture media after 7 days were outlined in Fig. 2C and D. Compared with the sterile medium, oral microbiota consistently reduced the corrosion potential E_{corr} and increased the corrosion current density i_{corr} of all the samples. The i_{corr} values reached 8.13 ± 0.9 μA cm^{-2}, 6.03 ± 1.1 μA cm^{-2}, 6.70 ± 0.6 μA cm^{-2} for subjects A, B, and C, which were all two orders of magnitude larger than that of abiotic control (0.06 ± 0.02 μA cm^{-2}). The average Epit value in the sterile medium was 626.6 ± 15.0 mV, whereas there was a significant decrease in Epit values of subject A (549.8 ± 62.3 mV), subject B (541.0 ± 80.0 mV), and subject C (560.0 ± 31.0 mV). However, no statistical difference was observed among the three groups in the presence of microbiota. The electrochemical data demonstrated again that the microbiota from all three subjects accelerated the corrosion of 316L SS. The different corrosivity of different microbiota was evident at almost all time points of electrochemical analyses and morphology observed by SEM and CLSM in Fig. 1. It was reasonable to speculate that these variations might be ascribed to the differences in the species composition of biofilms formed on the coupon surfaces. Fig. 2E–H shows the amount of metal ions (Fe, Cr, Ni, Mo) released by 316 L SS. Compared with the sterile group, although there was slight variation between subjects, the oral microbiota significantly increased the release of various metal ions. There was approximately 5–6 times Fe and 5–9 times Mo released in the presence of oral microbiota compared with the abiotic control. It was worth noting that the Cr ion released increased more than five folds and the Ni ion even reached 13–22 times more induced by the oral microbiota than the abiotic control, triggering a potential carcinogenic risk. Fig. S1 shows that in the presence of oral microbiota, the metal oxide composition of all elements on the coupon surface decreased, although slightly different in each group, the trends were consistent. This change supported the ion released data above.

3.3. 16S rRNA and metagenomic results

The oral microbiota compositions of original plankton and biofilm on 316 L SS after 7 days of co-culture from subjects A, B, and C were shown in the heatmap in Fig. 3A. The results of microbial diversity concurred with the morphological structure of the aforementioned SEM images of biofilm. Changes in the dominant genera were also observed among the groups. For subject A, *Streptococcus*, *Enterobacter,* and *Klebsiella* were prevalent, and *Lactobacillus* and *Rhodococcus* were the major species for subject B, while *Alcaligenaceae*, *Rhodococcus*, *Streptococcus*, *Bacillus*, *Devosia,* and *Stenotrophomonas* were abundant for subject C.

The PCoA analysis depicted in Fig. 3B illustrated that the spatial separation of samples along the coordinate axis corresponded to the diversity of flora between plankton and the biofilm on the coupon surface, demonstrating a significant divergence in the microbial community structures between those colonizing the material surface and those in the surrounding environment. Notably, the microbial community structure variations on the material surface were more pronounced than those among the planktonic microbial samples. For instance, subjects B and C were more similar in their biofilm microbial compositions, which were significantly different from subject A, which may lead to significantly different corrosion behaviors via a distinct microbial community structure because it was well known that biofilm was mainly responsible for MIC [20,21]. This suggested that the compositional differences in surface-attached biofilm rather than the planktonic in bulk might be a key factor influencing corrosion.

It has been reported [22] that corrosive microorganisms under anaerobic conditions usually contain acid-producing bacteria, sulfate-reducing bacteria, nitrate-reducing bacteria, and methanogenic archaea. Nitrogen, phosphorus, sulfur, and methane metabolic pathways were provided to identify the corrosion-related subgingival microbiota. As summarized from the metagenome results in Fig. 3C, nitrogen, and sulfur were endowed with the highest abundance of metabolism-related genes in subject A. Specifically, subject C had the highest phosphorus metabolism-related gene abundance. There were also significant differences in the abundance of sulfur and methane metabolism genes among the three groups. The initial exploration of the metagenome led us to further extract pathways related to ATP synthesis, carbon fixation, methane, nitrogen, and sulfur metabolism (Fig. S2). The results showed that the abundance of ATP synthesis pathways in subjects A and C was generally higher than that in subject B, except that the dominant pathways of the electron transport chain in subjects A and C were NADH/NADPH pathways and cytochrome-related pathways, respectively. Exploration of carbon fixation and methane metabolism pathways was closely related to the corrosion caused by the methanogens, and the results showed that subjects B and C possessed higher pathway abundance than subject A. The assimilating and disintegrating

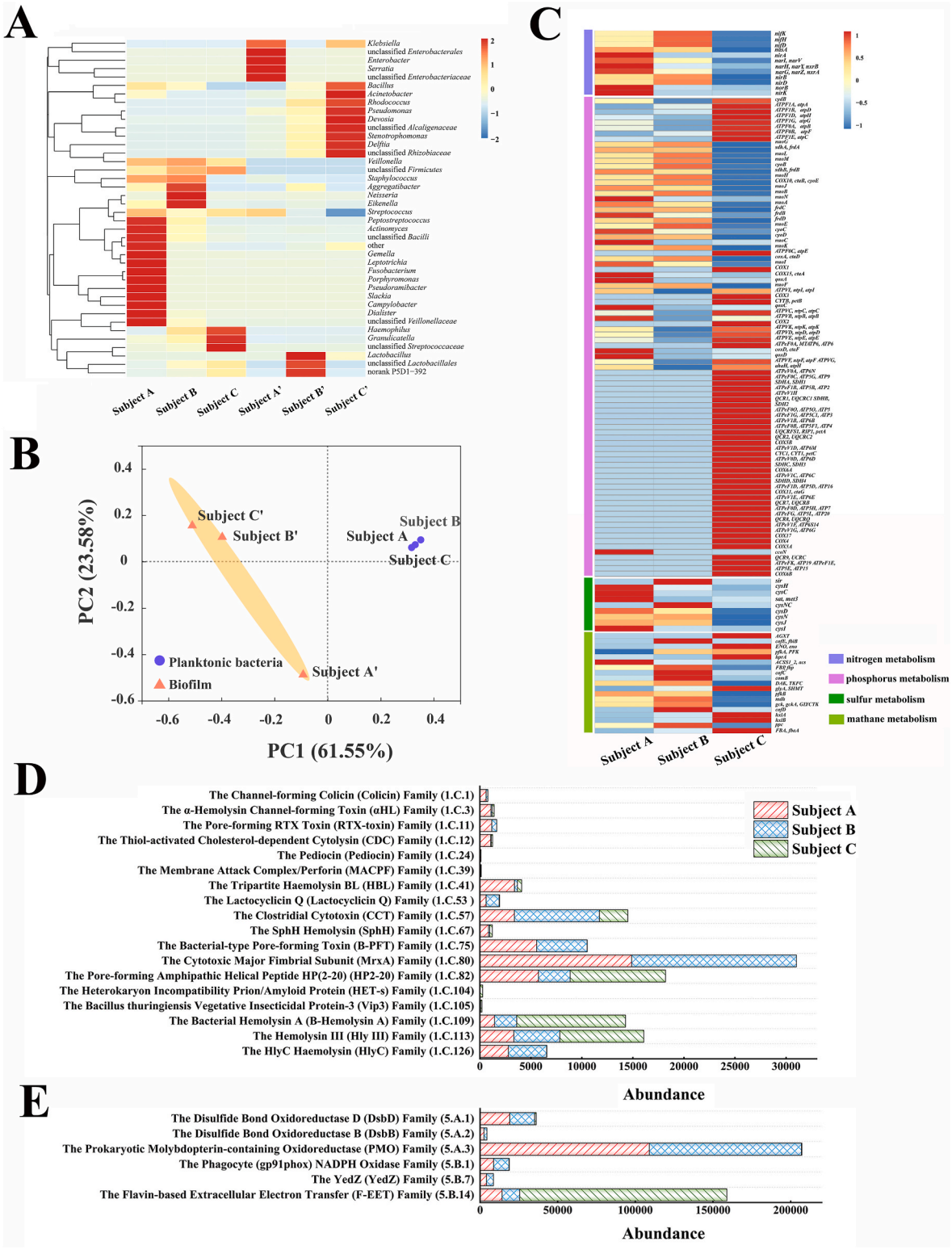

Fig. 3. 16S rRNA gene sequence results: (A) community heatmap analysis on genus level; (B) PCoA analysis on genus level. Functional gene abundance in metagenome: (C) heat map of nitrogen, phosphorus, sulfur and methane metabolism related gene abundance in metagenome; Pore-forming toxins (proteins and peptides) (D) and transmembrane electron carriers (E) gene abundance predicted by TCDB database.

effects of nitrate were higher in subject A than in subjects B and C, and we focused more on nitrate dissimilation, which could acquire electrons from metals and cause corrosion. Additionally, the dissimilation of sulfate also attracted attention; although relative abundance expression was slightly higher in subject A, absolute abundance was not prominent in the copy number. These results suggested that all three groups might contain different proportions of sulfate-reducing bacteria, while these sulfate-reducing bacteria were only accounted for a low proportion in the whole community and did not play a dominant role in the corrosion process. All the results above indicated that there were divergences in

the corrosion mechanisms for the three groups.

To explore the underlying MIC mechanisms among the three bacterial communities, we used the TCDB database to predict the expression of transmembrane electron carriers based on the metagenome (Fig. 3E), providing clues that help us to understand the potential corrosion mechanisms. The PMO family gene abundances in subjects A and B were high, while the gene abundance of the F-EET family in subject C was absolutely dominant. It has been reported that the PMO family can generate a proton motive force and transfer electrons across the membrane during anaerobic respiration, thereby having nitrate reduction ability [23].

The pore-forming toxins predicted by TCDB database in Fig. 3D indicated that different microbiota compositions might exert cytotoxic or genotoxic effects on human cells. The protein families with high expression abundance in the three groups included the clostridial cytotoxin (CCT) family (11.7 % relative abundance), pore-forming amphipathic helical peptide (HP2-20) family (14.7 % relative abundance), bacterial hemolysin A (B-Hemolysin A) family (11.5 % relative

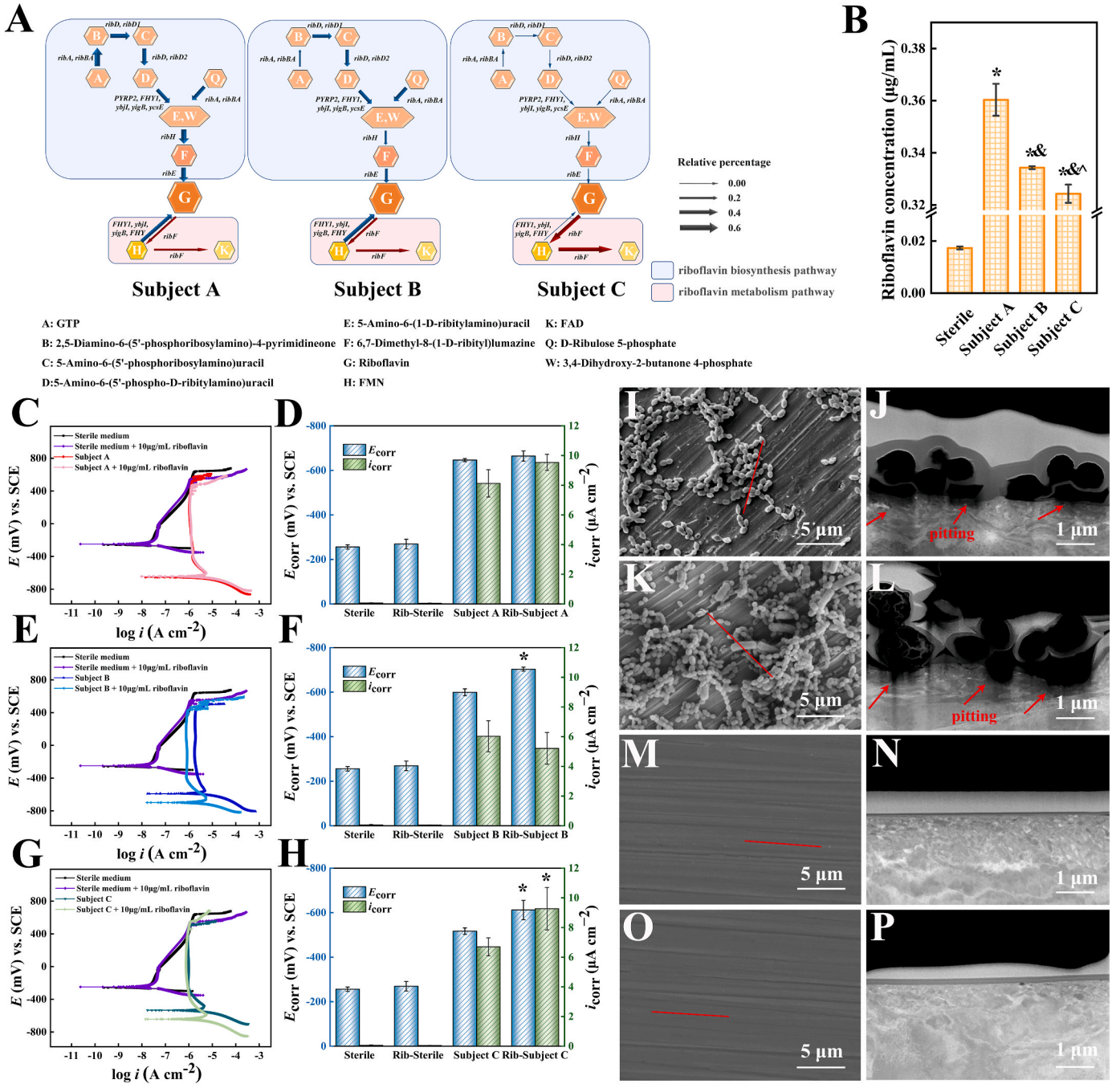

Fig. 4. Riboflavin accelerated corrosion of 316L SS in the presence of microbiota from subject C. Riboflavin biosynthesis and metabolic pathways related gene abundances in the metagenome (A). Concentrations of riboflavin after 7-day incubation (B). *: versus to sterile, $p < 0.05$; &: versus to subject A, $p < 0.05$; ^: versus to subject B, $p < 0.05$. Electrochemical analysis of 316L SS in different microflorae inoculated media with and without addition of riboflavin: the potentiodynamic polarization curves of subjects A (C), B (E) and C (G); fitted potentiodynamic polarization curves parameters of subjects A (D), B (F) and C (H). *: versus to without addition of riboflavin, $p < 0.05$. FIB-SEM/TEM characterization of 316L SS in the culture medium inoculated with microflorae from subject C with and without the addition of riboflavin. Subject C (I, J); subject C + 10 ppm riboflavin (K, L); sterile medium (M, N); sterile medium + 10 ppm riboflavin (O, P). The SEM morphology of the selected area (I, K, M, O); TEM observation of the passive film (J, L, N, P).

abundance), and hemolysin III (Hly III) family (12.9 % relative abundance). Meanwhile, in the expression of the cytotoxic major fimbrial subunit (MrxA) family, bacterial-type pore-forming toxin (B-PFT) family, and hemolysin (HlyC) family, the abundance displayed high-level of expression both in subjects A and B, while subject C group showed a lower level of expression. MrxA Family had the highest relative abundance among all pore-forming toxins families and reached nearly 25 %.

Our results confirmed that the oral microbiota significantly increased the release of various metal ions, which could affect the growth and metabolism of bacteria [24]. Bacteria could develop tolerance or resistance to heavy metal toxicity through self-regulation in response to environmental changes [24]. Fig. S3 showed the distinction of metal resistance gene abundance in the three bacterial communities. In general, subjects A and B shared similarities in the uniform abundance distribution. However, it showed a high concentration of distribution in individual genes in subject C. The results suggested that species diversity determined their functional properties.

3.4. Exogenous addition of riboflavin to verify EET-MIC

Flavins are potential electron shuttles, facilitating the EET-MIC of electroactive microbes [22]. The EET-MIC reactions of iron mediated by riboflavin [25] are as follows:

$$Fe^{0}+Flavin_{oxidized}\rightarrow Fe^{2+}+Flavin_{reduced}$$

$$Flavin_{reduced} + Microbe\ Electron\ Carrier_{oxidized}\rightarrow Flavin_{oxidized} + Microbe\ Electron\ Carrier_{reduced}$$

The biochemical source of flavin is riboflavin. According to the data of the metagenomic biosynthesis and metabolic pathways of riboflavin for three subjects (Fig. 4A), the gene abundance of the riboflavin synthesis pathway from high to low was represented by subjects A, B, and C, while the riboflavin metabolism pathway was just reversed. We observed a noticeable distinction in the metabolic and synthetic pathways for subjects A, B, and C, which was in accordance with the diverse riboflavin concentrations in the culture medium after 7 days (Fig. 4B). Subject A showed the highest riboflavin level of 0.36 μg/mL. The riboflavin concentrations in subjects B and C were 0.33 μg/mL and 0.32 μg/mL, respectively. Electrochemical experiments with the exogenous addition of 10 ppm riboflavin to the three groups were designed to verify whether the tested groups were electroactive. As shown in Fig. 4C–H and Fig. S4, riboflavin did not accelerate the abiotic corrosion of 316L SS, however, a significant accelerated corrosion was only observed when 10 ppm exogenous riboflavin was added to subject C. For subjects A and B, the corrosion current density showed no significant change after the addition of riboflavin. This result was consistent with the aforementioned predicted metabolic pathways of riboflavin, confirming that the microbiota from subject C was electroactive with the help of riboflavin.

As shown in Fig. S5, AES experiments with exogenous addition of riboflavin showed the changes of passive film on the surface of 316L SS in each group. The depth of the passive film was generally calculated according to the half of the sputtering depth change of O. Thus, the thickness of the passive film in subjects A, B, and C was reduced by 42 %, 23 %, and 20 %, respectively, compared with that in the sterile medium. When the exogenous addition of riboflavin was added to each group, no apparent differences in the thickness of passive film were observed in subjects A, B, and sterile medium. While in subject C, the passive film thickness of 316L SS was obviously thinned by exogenous riboflavin, about 29 %.

FIB-SEM/TEM was further employed to evaluate the passive film cocultured with microbiota from subject C with and without riboflavin (Fig. 4I–P). There was almost no change in the structure and thickness of the passive films before and after adding riboflavin to the sterile medium (Fig. 4M–P), supporting the electrochemical test data above. The 316 L SS in the presence of bacteria presented a clear and regular lattice phase without any amorphous-like microstructure between the matrix and biofilm, which intuitively explained that the passive film under the biofilm was destroyed (Fig. 4I–L). Specifically, more and deeper pit initiations appeared on the surface of 316 L SS with riboflavin addition in subject C (Fig. 4J and L).

3.5. Acids production from the microbiota to confirm M-MIC

Acids secreted from the microbiota can be another main contributor to the corrosion of 316L SS. Therefore, the concentrations of different acids were detected in each group. As shown in Fig. 5A, after 7 days of coculture, PO_4^{3-}, Cl^-, and SO_4^{2-} inorganic ions in the bacterial media were significantly increased compared with those in the sterile medium. Among them, the concentration of PO_4^{3-} in subject C reached 1017 μg/mL, significantly higher than those in subject A (849 μg/mL) and B (889 μg/mL), which echoed the results of the phosphorus metabolism gene abundance in the metagenome. Fig. 5B shows the results of the concentrations of the secreted organic acids. As the main product of anaerobic fermentation, the lactic acid concentration was significantly higher than the other organic acids in each group. Subjects B and C had similar concentrations (3733 μg/mL and 3682 μg/mL, respectively), roughly four times more than that of subject A (833 μg/mL). There was no change in the pH of the sterile medium over time (Fig. 5C). Subjects B and C showed a similar pattern, a sharp decrease to 4.4 on the first day and then a nearly stable value afterward. The pH of subject A decreased to 5.9 on the first day and then gradually increased to 6.7 on the seventh day, which was close to the sterile medium.

4. Discussion

The formation of biofilms is a highly spontaneous process that alternates growth and extinction and changes continuously with the environment. The species and abundance of the initial planktonic microorganisms showed similarities with the common dominant bacterial genera in the oral cavity. For example, common constituents of the oral microbiome, such as *Veillonococcus*, *Streptococcus,* and *Enterobacter*, could be detected in all groups. The microecological environment of diverse microorganisms may greatly alter their physiological characteristics, as manifested from several previous studies, such as given the ability of anaerobic bacteria to survive in the aerobic environment [26], and the metabolites of the same microorganism within different environments may change significantly [27]. Then, the exploration of the target physiology of microbiota requires a thorough understanding of the specific environment as well as the coexisting surrounding neighbors. We made a multifaceted comparison of the biofilms of different subjects, and the changes in planktonic bacteria and biofilm on the coupon surface in the same subject were observed. The microbiota of each subject presented a diverse and unique microecological environment, and the planktonic bacteria and biofilm on the coupon surface in the same subject were also significantly different.

From the pH results, we found that the changes in pH value were not consistent with the electrochemical results. One possible explanation might be the pH value we obtained was that in the bulk media rather than the pH underneath the biofilm. The dense biofilm formed on the coupon surface might impede the diffusion of acidic metabolites, leading to a lower localized pH value underneath the biofilm than that in the bulk media, which needed further validation [28]. In our previous report, we found that the corrosivity of 316L SS in the abiotic medium at pH 3.3 was slightly stronger than those at pH 4.3 and 5.3, but significantly smaller than those in the presence of *Streptococcus mutans* biofilms, confirming again that biofilm was the key contributor to corrosion rather than the bulk pH [11]. The results indicated that the acidic environment produced by the metabolites of oral subgingival microbiota might be one of the reasons for corrosion, confirming the existence of M-MIC. However, it was reasonable to speculate that EET-MIC may contribute more to the whole corrosion process because subject A caused the most severe corrosion without the lowest pH.

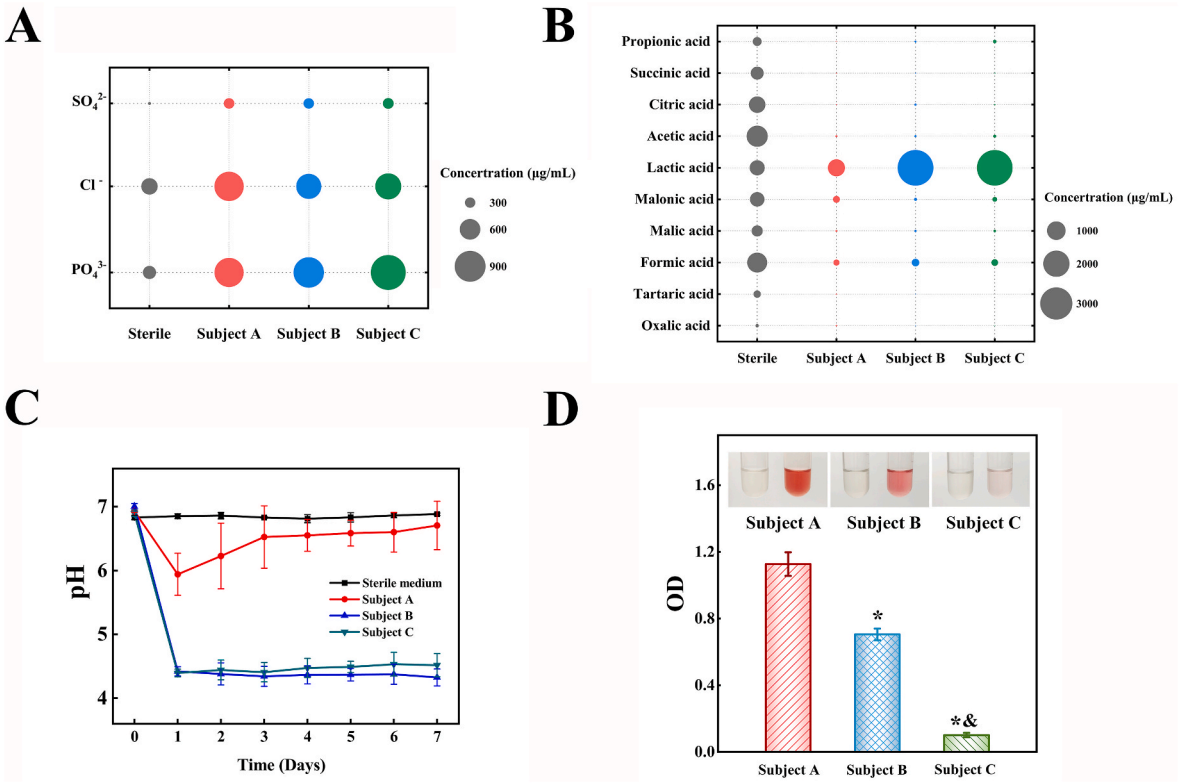

Fig. 5. The concentrations of major inorganic acid ions (A), the concentrations of organic acids (B) and pH values (C) in the different media, the absorbance value at 538 nm in Griess nitrate reduction test (D). *: versus to subject A, $p < 0.05$; &: versus subject B, $p < 0.05$.

The predicted metagenomic data with the TCDB database found that transmembrane electron carriers existed in all three bacterial communities. However, the types of electron transfer carriers were different. The PMO family gene abundance in subjects A and B was high, while the gene abundance of the F-EET family in subject C was absolutely dominant. The high expression of the F-EET family in subject C proved that this microbiota had the ability of extracellular electron transfer based on flavin. Flavin mononucleotide (FMN) and flavin adenine dinucleotide (FAD) are collectively referred to as flavins [29]. For electron transporters of flavins, it was believed in early studies that they could be secreted using an efflux-type transporter by bacteria and shuttled back and forth between electrodes and bacteria through diffusion in the form of a free state, thus promoting the EET process [30–32]. A recent study has shown that flavin molecules secreted by *Shewanella oneidensis* MR-1 can enhance the ability of outer-surface *c*-type cytochrome to transport electrons as redox cofactors and accelerate EET processes in the form of complexes [33]. Light et al. [34] observed that EET activation correlated with cellular NADPH dehydrogenase and NAD^+ levels, which was consistent with our finding as shown in Fig. S2 that subject C was highly expressed in the NADPH dehydrogenase pathway. FMN was also injected into an *L. monocytogenes*-inoculated electrochemical chamber, resulting in a pronounced increase in electric current [33]. The biochemical source of flavin is riboflavin [29], and the results in Fig. 4A and B revealed that the highest riboflavin concentration in the medium of subject A was due to the highest abundance of the synthetic pathway and the lowest gene abundance of the metabolic pathway of riboflavin. Contrary to the result of subject A, the lowest riboflavin synthesis pathway gene abundance and the highest riboflavin metabolism pathway gene abundance in subject C resulted in the lowest riboflavin concentration in the medium of subject C among the three groups. Riboflavin synthesis and metabolism occurred intracellularly, and subject C might consume most of the produced riboflavin within the cells because of its strong riboflavin consumption ability. Only riboflavin secreted extracellularly played an important role in improving the electron transfer efficiency, thus increased corrosion current density after the exogenous addition of riboflavin to subject C indicated that subject C did not secret a sufficient amount of riboflavin extracellularly. This result corresponded to the characteristic flavin-based extracellular electron transfer ability of subject C in Fig. 3E. Of course, riboflavin can also be the growth factor or the nutrient source for other microorganisms.

Nitrate concentration is another important indicator for EET-MIC, because nitrate reducing bacteria can couple iron oxidation with nitrate reduction, thus accelerating MIC [35]. The reduction reactions are listed as follows:

$$2NO_3^- + 10e^- + 12H^+ \rightarrow N_2 + 6H_2O;$$

$$NO_3^- + 8e^- + 10H^+ \rightarrow NH_4^+ + 3H_2O$$

Previous studies on nitrate-reducing bacteria showed that they could directly uptake electrons from the steel surface, and the corrosivity was even greater than that of sulfate-reducing bacteria [36]. It is well known that nitrate commonly appears in oral saliva. Therefore a Griess assay was performed to verify whether the microbiota had nitrate reduction ability. As shown in Fig. 5D, a visible color change was observed, and the absorbance value at 538 nm indicated statistically significant differences in pairwise comparisons of the three groups. The OD values of subjects A, B, and C from high to low showed that subjects A and B released a large amount of nitrite. In contrast, only a small amount of nitrite was produced by subject C. The POM family (Fig. 3E) can generate a proton motive force and transfer electrons across the membrane during anaerobic respiration, thereby having nitrate reduction ability. Our result was consistent with the higher nitrate reduction pathway abundance obtained in Fig. S2. It was proven that subjects A and B displayed high nitrate reduction capacity, which may also contribute to EET-MIC.

When oral subgingival bacteria colonized the surface of 316 L SS, a large amount of metal ions were released due to microbial corrosion. Affected by environmental influences, microbiota inevitably produces

corresponding feedback [25]. When environmental metal ions were essential metal trace elements for bacterial growth and metabolism, the initial response of bacteria was to increase the intake of metal ions, which was conducive to the bioactivities of bacteria and as ion reserves [37,38]. For example, highly expressed ModABC in subjects A and B (Fig. S3D) was reported to be a critical membrane-bound transporter for molybdenum ion intake, molybdenum took part in the formation of active sites of various enzymes, molybdoenzymes catalyzed various oxidation/reduction reactions, and participated in the metabolism of nitrogen, carbon, and sulfur [38]. The highly expressed corA family of subject C in Fig. S3C was a substantial membrane uptake or transport system of nickel in bacteria [39]. If the heavy metal ion concentration exceeds a certain threshold, deleterious or pleiotropic effects may be observed [25,40]. Microbial flora would have developed numerous mechanisms for maintaining the dynamic balance of metal ions required through a range of physiological processes, thus producing tolerance or resistance to the influence of heavy metal ions [25,41]. Such as NfsA in Fig. S3B could reduce chromate to soluble and hypotoxic Cr(III) to attenuate cell damage [42]. It was worth noting that in Fig. S3C, ArsA and ArsB, which were highly abundant in subjects A and B, together formed a two-component membrane system. ArsA functioned as an ATPase, and ArsB was a transmembrane protein, which collectively formed a transmembrane channel for the transport of metal ions from the cytoplasm [43]. Likewise, ArsR was a metalloregulatory transcriptional repressor that sensed various heavy metal ions in cells and then removed them from the cytoplasm [44]. The metal resistance genes showed a divergent expression pattern among the three groups in Fig. S3, which indicated that the sensitivity and response ability to heavy metal ions was different due to the varied corrosion behaviors and mechanisms of each group.

Dynamic changes in the microbiota would be closely associated with the surrounding tissue physiological state of the host [45]. According to the etiology of peri-implantitis, we analyzed pore-forming toxins (proteins and peptides) in metagenomes. Pore-forming toxins were synthesized and secreted by pathogenic bacteria, usually destroyed the host cell membrane and formed transmembrane pores, which allowed for the passage of electrolytes and other small molecules, even pathogenic microorganisms, directly and freely, leading to the degradation and demise of the target cell via necrotic and apoptotic mechanisms [45–48]. Studies have shown that the dissolution of nickel and chromium ions caused by metal corrosion might induce undesirable effects such as induced allergic reactions, oxidative stress, cytotoxicity, and genotoxicity [25,39,40]. It was reasonable to speculate that the immune barrier of the host was destroyed by pore-forming toxins, which further amplified the adverse health effects of ion release caused by corrosion. Therefore, our findings suggested that more forward-looking options [49–51], including corrosion-resistant biofunctional materials and efficient therapeutic methods, could be chosen clinically to prevent the potential negative effect caused by oral microbial corrosion.

5. Conclusion

Multispecies biofilms with complex structures were formed by the oral subgingival microbiota on 316L SS surfaces in the simulated oral anaerobic environment, significantly accelerating the corrosion of 316L SS in the form of pitting. There were obvious disparities in biofilm composition, corrosion behaviors, and mechanisms among microbiota samples collected from the subjects. A significant divergence in the microbial community structures between biofilms and planktons from three subjects was observed. Subject A's biofilm composition was significantly different from those of subjects B and C, leading to their different corrosion rates and mechanisms. M-MIC by acidic metabolites contributed to the MIC process, and EET-MIC played an essential role in accelerating corrosion via electron shuttle riboflavin and nitrate reduction pathways. Exogenous addition considerably facilitated the corrosion of subject C, while nitrate reduction was more favorable for the MIC of subjects A and B. Our findings obtained via interdisciplinary techniques of material science and bioinformatics shed light on the understanding of the underlying mechanisms of oral microbial corrosion. Because of the complexity of the interactions among materials, microorganisms, and the oral environment, further in-depth oral microbial corrosion mechanism investigations are desired.

CRediT authorship contribution statement

Ying Zheng: Writing – original draft, Project administration, Methodology, Investigation, Formal analysis, Data curation. **Yi Yang:** Methodology, Investigation, Formal analysis, Data curation, Conceptualization. **Xianbo Liu:** Writing – review & editing, Formal analysis. **Pan Liu:** Formal analysis, Data curation. **Xiangyu Li:** Investigation. **Mingxing Zhang:** Writing – review & editing, Data curation. **Enze Zhou:** Writing – review & editing. **Zhenjin Zhao:** Resources. **Xue Wang:** Resources. **Yuanyuan Zhang:** Resources. **Bowen Zheng:** Investigation. **Yuwen Yan:** Methodology. **Yi Liu:** Conceptualization. **Dake Xu:** Writing – review & editing, Project administration, Methodology, Conceptualization. **Liu Cao:** Conceptualization.

Declaration of competing interest

The authors declare no competing interests.

Acknowledgments

This work was supported by grants from the National Key Research and Development Program of China (2020YFA0907300), the National Natural Science Foundation of China (Nos. U2006219 and 51871050), the Fundamental Research Funds for the Central Universities (Nos. N180203019 and N2002019), Liaoning Revitalization Talents Program (No. XLYC1907158), and Basic Scientific Research Project of Education Department of Liaoning Province and Shenyang Young and middle-aged Scientific and Technological Innovation Talents Support Program (RC210001).

Appendix A. Supplementary data

Supplementary data to this article can be found online at https://doi.org/10.1016/j.bioactmat.2024.01.007.

References

[1] W. Dou, D. Xu, T. Gu, Biocorrosion caused by microbial biofilms is ubiquitous around us, Microb. Biotechnol. 14 (2021) 803–805.
[2] N. Kip, J.A. van Veen, The dual role of microbes in corrosion, ISME J. 9 (2015) 542–551.
[3] M. Dzidic, M.C. Collado, T. Abrahamsson, A. Artacho, M. Stensson, M.C. Jenmalm, et al., Oral microbiome development during childhood: an ecological succession influenced by postnatal factors and associated with tooth decay, ISME J. 12 (2018) 2292–2306.
[4] D. Perera, A. McLean, V. Morillo-López, K. Cloutier-Leblanc, E. Almeida, K. Cabana, et al., Mechanisms underlying interactions between two abundant oral commensal bacteria, ISME J. 16 (2022) 948–957.
[5] Y.H. Lee, S.W. Chung, Q.S. Auh, S.J. Hong, Y.A. Lee, J. Jung, et al., Progress in oral microbiome related to oral and systemic diseases: an update, Diagnostics 11 (2021) 1283.
[6] Y. Hao, X. Huang, X. Zhou, M. Li, B. Ren, X. Peng, et al., Influence of dental prosthesis and restorative materials Interface on Oral Biofilms, Int. J. Mol. Sci. 19 (2018) 3157.
[7] J. Mystkowska, K. Niemirowicz-Laskowska, D. Lysik, G. Tokajuk, J.R. Dabrowski, R. Bucki, The role of oral cavity biofilm on metallic biomaterial surface destruction-corrosion and friction aspects, Int. J. Mol. Sci. 19 (2018) 743.
[8] L. Li, S. Li, Q. Qu, L. Zuo, Y. He, B. Zhu, et al., *Streptococcus sanguis* biofilm architecture and its influence on titanium corrosion in enriched artificial saliva, Materials 10 (2017) 255.
[9] M.A. De la Garza-Ramos, F.H. Estupinan-Lopez, C. Gaona-Tiburcio, L.G. Beltran-Novelo, P. Zambrano-Robledo, J. Cabral-Miramontes, et al., Electrochemical behavior of Ti6Al4V alloy used in dental implants immersed in *Streptococcus gordonii* and *Fusobacterium nucleatum* solutions, Materials 13 (2020) 4185.

[10] J. Mystkowska, Biocorrosion of dental alloys due to *Desulfotomaculum nigrificans* bacteria, Acta Bioeng. Biomech. 18 (2016) 87–96.
[11] Y. Yang, M. Masoumeh, E. Zhou, D. Liu, Y. Song, D. Xu, et al., *Streptococcus mutans* biofilms induce metabolite-mediated corrosion of 316 L stainless steel in a simulated oral environment, Corrosion Sci. 182 (2021) 109286.
[12] K. Becker, A. Pliska, C. Busch, B. Wilmes, M. Wolf, D. Drescher, Efficacy of orthodontic mini implants for en masse retraction in the maxilla: a systematic review and meta-analysis, Int. J. Implant Dent. 4 (2018) 35.
[13] J.C. Francis, U. Oz, L.L. Cunningham, P. Emecen Huja, R.J. Kryscio, S.S. Huja, Screw-type device diameter and orthodontic loading influence adjacent bone remodeling, Angle Orthod. 87 (2017) 466–472.
[14] P. Mecenas, D.G. Espinosa, P.C. Cardoso, D. Normando, Stainless steel or titanium mini-implants? Angle Orthod. 90 (2020) 587–597.
[15] Q. Wang, M. Zhang, C. Yang, Y. Yang, E. Zhou, P. Liu, et al., Oral microbiota accelerates corrosion of 316L stainless steel for orthodontic applications, J. Mater. Sci. Technol. 128 (2022) 118–132.
[16] T. Zheng, J. Li, Y. Ji, W. Zhang, Y. Fang, F. Xin, et al., Progress and prospects of bioelectrochemical systems: electron transfer and its applications in the microbial metabolism, Front. Bioeng. Biotechnol. 8 (2020) 10.
[17] U. Gopalakrishnan, A.S. Felicita, L. Mahendra, M.A. Kanji, S. Varadarajan, A.T. Raj, et al., Assessing the potential association between microbes and corrosion of intra-oral metallic alloy-based dental appliances through a systematic review of the literature, Front. Bioeng. Biotechnol. 9 (2021) 631103.
[18] S. Wakai, N. Eno, H. Mizukami, T. Sunaba, K. Miyanaga, Y. Miyano, Microbiologically influenced corrosion of stainless steel independent of sulfate-reducing bacteria, Front. Microbiol. 13 (2022) 982047.
[19] H.Y. Tang, C. Yang, T. Ueki, C.C. Pittman, D. Xu, T.L. Woodard, et al., Stainless steel corrosion via direct iron-to-microbe electron transfer by *Geobacter* species, ISME J. 15 (10) (2021) 3084–3093.
[20] D. Xu, T. Gu, D.R. Lovley, Microbially mediated metal corrosion, Nat. Rev. Microbiol. 21 (2023) 705–718.
[21] Y. Jin, E. Zhou, T. Ueki, D. Zhang, Y. Fan, D. Xu, et al., Accelerated microbial corrosion by magnetite and electrically conductive pili through direct Fe^0 -to-Microbe electron transfer, Angew Chem. Int. Ed. Engl. 62 (38) (2023) e202309005.
[22] B.J. Baker, V. De Anda, K.W. Seitz, N. Dombrowski, A.E. Santoro, K.G. Lloyd, Diversity, ecology and evolution of Archaea, Nat Microbiol 5 (7) (2020) 887–900.
[23] R.A. Rothery, G.J. Workun, J.H. Weiner, The prokaryotic complex iron-sulfur molybdoenzyme family, Biochim. Biophys. Acta 1778 (2008) 1897–1929.
[24] Z. Ma, F.E. Jacobsen, D.P. Giedroc, Coordination chemistry of bacterial metal transport and sensing, Chem. Rev. 109 (2009) 4644–4681.
[25] E. Zhou, F. Li, D. Zhang, D. Xu, Z. Li, R. Jia, et al., Direct microbial electron uptake as a mechanism for stainless steel corrosion in aerobic environments, Water Res. 219 (2022) 118553.
[26] F.E. Dewhirst, T. Chen, J. Izard, B.J. Paster, A.C. Tanner, W.H. Yu, et al., The human oral microbiome, J. Bacteriol. 192 (2010) 5002–5017.
[27] I. Rabbers, J.H. van Heerden, N. Nordholt, H. Bachmann, B. Teusink, F. J. Bruggeman, Metabolism at evolutionary optimal States, Metabolites 5 (2015) 311–343.
[28] H. Feng, X. Zhang, G. Wu, W. Jin, Q. Hao, G. Wang, et al., Unusual anti-bacterial behavior and corrosion resistance of magnesium alloy coated with diamond-like carbon, RSC Adv. 6 (2016) 14756–14762.
[29] C.A. Abbas, A.A. Sibirny, Genetic control of biosynthesis and transport of riboflavin and flavin nucleotides and construction of robust biotechnological producers, Microbiol. Mol. Biol. Rev. 75 (2011) 321–360.
[30] E. Marsili, D.B. Baron, I.D. Shikhare, D. Coursolle, J.A. Gralnick, D.R. Bond, *Shewanella* secretes flavins that mediate extracellular electron transfer, Proc. Natl. Acad. Sci. U. S. A. 105 (2008) 3968–3973.
[31] E.D. Brutinel, A.M. Dean, J.A. Gralnick, Description of a riboflavin biosynthetic gene variant prevalent in the phylum *Proteobacteria*, J. Bacteriol. 195 (2013) 5479–5486.
[32] N.J. Kotloski, J.A. Gralnick, Flavin electron shuttles dominate extracellular electron transfer by *Shewanella oneidensis*, mBio 4 (2013) e00553-12.
[33] A. Okamoto, K. Hashimoto, K.H. Nealson, R. Nakamura, Rate enhancement of bacterial extracellular electron transport involves bound flavin semiquinones, Proc. Natl. Acad. Sci. U. S. A. 110 (2013) 7856–7861.
[34] S.H. Light, L. Su, R. Rivera-Lugo, J.A. Cornejo, A. Louie, A.T. Iavarone, et al., A flavin-based extracellular electron transfer mechanism in diverse gram-positive bacteria, Nature 562 (2018) 140–144.
[35] D. Xu, Y. Li, F. Song, T. Gu, Laboratory investigation of microbiologically influenced corrosion of C1018 carbon steel by nitrate reducing bacterium *Bacillus licheniformis*, Corrosion Sci. 77 (2013) 385–390.
[36] S. Lahme, D. Enning, C.M. Callbeck, D. Menendez Vega, T.P. Curtis, I.M. Head, et al., Metabolites of an oil field sulfide-oxidizing, nitrate-reducing *sulfurimonas* sp. cause severe corrosion, Appl. Environ. Microbiol. 85 (3) (2019) e01891-18.
[37] J.M. Moulis, Cellular dynamics of transition metal exchange on proteins: a challenge but a bonanza for coordination chemistry, Biomolecules 10 (2020) 1548.
[38] X. Ge, M.P. Thorgersen, F.L. Poole 2nd, A.M. Deutschbauer, J.M. Chandonia, P. S. Novichkov, et al., Characterization of a metal-resistant Bacillus strain with a high molybdate affinity ModA from contaminated sediments at the oak ridge reservation, Front. Microbiol. 11 (2020) 587127.
[39] A. Stetsenko, A. Guskov, Cation permeability in CorA family of proteins, Sci. Rep. 10 (2020) 840.
[40] S. Latvala, J. Hedberg, S. Di Bucchianico, L. Moller, I. Odnevall Wallinder, K. Elihn, et al., Nickel release, ROS generation and toxicity of Ni and NiO micro- and nanoparticles, PLoS One 11 (2016) e0159684.
[41] X. Hao, J. Zhu, C. Rensing, Y. Liu, S. Gao, W. Chen, et al., Recent advances in exploring the heavy metal(loid) resistant microbiome, Comput. Struct. Biotechnol. J. 19 (2021) 94–109.
[42] D.F. Ackerley, C.F. Gonzalez, M. Keyhan, R. Blake 2nd, A. Matin, Mechanism of chromate reduction by the *Escherichia coli* protein, NfsA, and the role of different chromate reductases in minimizing oxidative stress during chromate reduction, Environ. Microbiol. 6 (2004) 851–860.
[43] R. Castillo, M.H. Saier, Functional promiscuity of homologs of the bacterial ArsA ATPases, Internet J. Microbiol. 2010 (2010) 187373.
[44] R. Rawle, T.C. Saley, Y.S. Kang, Q. Wang, S. Walk, B. Bothner, et al., Introducing the ArsR-regulated arsenic stimulon, Front. Microbiol. 12 (2021) 630562.
[45] I. Iacovache, M. Bischofberger, F.G. van der Goot, Structure and assembly of pore-forming proteins, Curr. Opin. Struct. Biol. 20 (2010) 241–246.
[46] M. Bischofberger, I. Iacovache, F.G. van der Goot, Pathogenic pore-forming proteins: function and host response, Cell Host Microbe 12 (2012) 266–275.
[47] M. Dal Peraro, F.G. van der Goot, Pore-forming toxins: ancient, but never truly out of fashion, Nat. Rev. Microbiol. 14 (2016) 77–92.
[48] H. Ostolaza, D. Gonzalez-Bullon, K.B. Uribe, C. Martin, J. Amuategi, X. Fernandez-Martinez, Membrane permeabilization by pore-forming RTX toxins: what kind of lesions do these toxins form? Toxins 11 (2019) 354.
[49] Z. Li, E. Wang, Y. Zhang, R. Luo, Y. Gai, H. Ouyang, et al., Antibacterial ability of black titania in dark: via oxygen vacancies mediated electron transfer, Nano Today 50 (2023) 101826.
[50] S.M.J. Moghadas, M. Yeganeh, S.R.A. Zaree, M. Eskandari, Influence of low temperature heat treatment on microstructure, corrosion resistance and biological performance of 316L stainless steel manufactured by selective laser melting, CIRP J Manuf Sci Technol 40 (2023) 68–74.
[51] M. Yeganeh, M.H. Rezvani, S.M. Laribaghal, Electrochemical behavior of additively manufactured 316L stainless steel in H_2SO_4 solution containing methionine as an amino acid, Colloids Surf., A 627 (2021) 127120.